Applied Petrochemical Research (2018) 8:39–53
https://doi.org/10.1007/s13203-018-0196-7

ORIGINAL ARTICLE

Response surface models for synthetic jet fuel properties

R. L. J. Coetzer[1,4] · T. S. Joubert[2,3] · C. L. Viljoen[2] · R. J. J. Nel[2] · C. A. Strydom[3]

Received: 30 November 2017 / Accepted: 23 February 2018 / Published online: 9 March 2018

Abstract
Jet fuel is a mixture of different hydrocarbon groups, and the mass contribution of each of these groups toward the overall chemical composition of the fuel dictates the bulk physical properties of the fuel after completion of the refining and blending processes. The fluidity properties of jet fuel mixtures at low temperatures are critical in understanding and mitigating the safety risks and performance attributes of aircraft engines, which may lead to the introduction of more stringent specification limits in the near future. Therefore, in this study the low-temperature viscosity and freeze point properties of jet fuels were investigated by variation of the linear to branched chain paraffin mass ratio, in conjunction with variation of the carbon number distribution according to a mixture by process variables experimental design. Furthermore, response surface models were developed and discussed for the two main fluidity properties of interest and inferences were made from the models for the potential generation of optimal jet fuel mixtures.

Keywords Freeze point · Mixture experimental designs · Response surface models · Synthetic jet fuel · Viscosity

Introduction

Since the introduction of turbine powered aircraft approximately 70 years ago, the aviation industry has grown from a novelty to an essential need [1]. According to Schäfer [2], air transportation currently accounts for approximately 10% of the passenger kilometres travelled by all motorised modes, and for nearly 40% of the interregional transport of goods by value. The aviation industry consequently produces 700 m tonnes of CO_{2eq} annually, which accounts for approximately 12% of global transportation emissions. Environmentally friendly (low sulphur and aromatic content) fuels are hence desired; these consist primarily of *n*- and iso-paraffins, as well as cycloparaffins, as they produce less emissions [3].

✉ T. S. Joubert
tertius.joubert@sasol.com

1 Sasol Group Technology, 1 Klasie Havenga Road, Sasolburg 1947, South Africa

2 Sasol Energy Technology, 1 Klasie Havenga Road, Sasolburg 1947, South Africa

3 Chemical Resource Beneficiation, North-West University, Potchefstroom Campus, Private Bag X6001, Potchefstroom 2520, South Africa

4 University of the Free State, Box 339, Bloemfontein 9300, South Africa

Furthermore, conventional crude oil derived jet fuel is also becoming more expensive due to volatile markets [4]. The aforementioned environmental and cost factors, in combination with aspects such as energy security and the continued availability of crude oil, have placed renewed focus on the development of alternative/synthetic jet fuels by industry role players. These synthetic jet fuels are produced from biomass resources such as fermentation sugars, lignocellulosic feedstocks, triglyceride oils, algae, and seaweed [5].

Fischer–Tropsch refining

Fischer–Tropsch (F–T) refineries utilise mixtures of carbon monoxide (CO) and hydrogen (H_2), named synthesis gas, to produce synthetic liquid fuels. The synthesis gas can be obtained from virtually any carbon source. The most widely used materials for synthesis gas production are [6]:

- Coal: coal-to-liquids (CTL);
- natural gas: gas-to-liquids (GTL); and
- biomass: biomass-to-liquids (BTL).

In order to convert feed materials into jet fuel, three fundamental process steps are employed, namely synthesis gas production, F–T synthesis, and refining [7]. In the first step, synthesis gas (CO and H_2) is produced by gasification or

reforming of the feed material. Impurities are then removed from the synthesis gas, whereafter it is routed to the F–T reactor for the production of synthetic crude oil. In the final step, the synthetic crude oil is refined to produce various products, including jet fuel.

Products produced by Fischer–Tropsch synthesis are considered more environmentally friendly than their crude oil counterparts, as such products contain no sulphur, or metals, and consist mainly of linear paraffins and branched paraffins [8]. The presence of aromatic compounds in these fuels depends on the type of Fischer–Tropsch technology employed during the refining process.

Jet fuel fluidity

For the past 60 years the freeze point specification of jet fuel was considered the most important property to ensure that jet fuels in the market were fit for use. However, aviation industry Original Equipment Manufacturers (OEMs), along with the Coordinating Research Council (CRC), established that appropriate fuel atomisation within the aircraft's Auxiliary Power Unit (APU) can only occur at fuel viscosities not exceeding 12 cSt [9]. It was further discovered that some jet fuels currently in the market may exceed the 12 cSt viscosity threshold as the fuel approaches the freeze point specification maximum. As a result of the concerns raised by the CRC as well as aviation industry OEMs, ASTM International (the entity who governs international jet fuel specifications) is currently investigating the validity of these claims, as well as means to mitigate this risk [10].

It is anticipated that the focus on fluidity of jet fuel at low temperatures will increase in the near future and that more stringent specifications may be applied to jet fuel products. The effect of molecular branching and carbon number distribution on the low-temperature fluidity characteristics of F–T derived synthetic jet fuel in the C_9–C_{18} carbon number range was thus investigated to gain a better understanding of these relationships.

In this paper, the statistical mixture by process variable design of experiments is presented and applied to study the viscosity and freeze point properties of synthetic jet fuel, by variation of the branched to linear paraffin (*i*:*n*) mass ratio, in conjunction with variation of the carbon number distribution. Furthermore, the statistical design by response surface modelling methodology employed to develop accurate predictive models for the low temperature fluidity characteristics is discussed in detail.

The paper is outlined as follows. The experimental data and the statistical design of experiments are discussed in "Experimental data and the statistical design of experiments". Development of the response surface models are also presented in "Experimental data and the statistical design of experiments". The response surface models for the fluidity characteristics are discussed in "Statistical models and discussion", together with detailed interpretations. In "Optimization studies" some optimization studies are presented for specifying the optimum jet fuel blends in order to satisfy specific targets for the freeze point and viscosity of the blend. The conclusions that were reached are discussed in "Conclusion".

Experimental data and the statistical design of experiments

Refinery streams

Typical F–T refinery product streams were chosen as mixture components for the study; one stream was rich in *n*-paraffins, whereas the other was rich in iso-paraffins. The *n*-paraffin feedstock was obtained from Arbeitsgemeinschaft Ruhrchemie-Lurgi (Arge) Low Temperature Fischer–Tropsch (LTFT) synthesis. The *n*-paraffin content of the Arge LTFT feedstock was ± 90%, which corresponds well to the values reported by de Klerk in 2008 [11]. The product stream rich in iso-paraffins was also obtained from LTFT synthesis; however, this feedstock was highly isomerised to produce a product that consisted of ± 90% iso-paraffins. These refinery streams were consequently separated into individual *n*- and iso-paraffin carbon number mixture components in the C_9–C_{18} carbon number range by means of a 30 theoretical plate fractional distillation unit. The resultant mixture components were characterised using a two-dimensional gas chromatography system (GC × GC), equipped with both a Time-of-Flight Mass Spectrometer (TOF–MS) and a flame ionisation detector (FID), to determine the suitability of each component for use in the study. The compositions of the *n*- and iso-paraffin mixture components are depicted in Figs. 1, 2, respectively. The *n*- and iso-paraffin mixture components did contain smaller quantities of undesired components; however, these mixture components were still deemed fit for use in the study.

In order to better understand the effect of molecular branching and carbon number distribution on the viscosity and freeze point properties of synthetic jet fuel, it was required to prepare mixtures consisting of different *i*:*n* mass ratios and carbon number distributions. The statistical design of experiments was employed for specifying the optimal set of blends to achieve the objectives of this study. The freeze point of each blend was measured using a Phase Technology® FP-70X freeze point analyser conforming to the requirements of the ASTM D5972 method. In turn, the viscosity of each blend was determined by an Anton Paar Stabinger SVM 3000 viscometer that conformed to the requirements of the ASTM D7042 method.

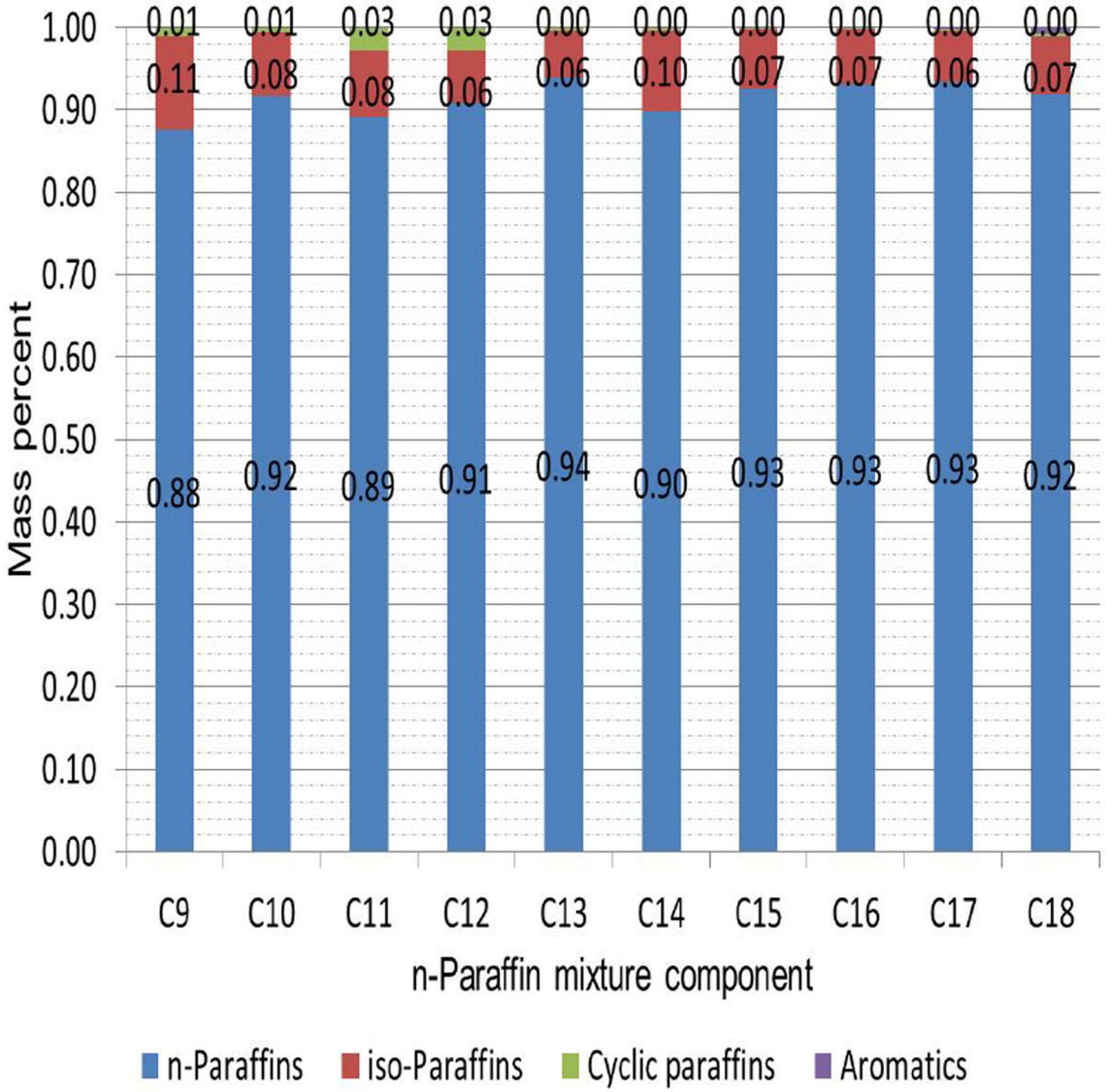

Fig. 1 Compositional graph of *n*-paraffin GC × GC results

Model building

Specification of the mixtures to obtain sufficient experimental data for statistical model development is not a trivial exercise. More specifically, the experimental study of the *i*:*n* mass ratios and carbon number distribution is a mixture by mixture variables problem. Cornell [12] provides a comprehensive overview of the design of experiments in mixture variables and model development. Mixture variables are naturally constrained between 0 and 1 and add up to a fixed total, say 1 (total mass fraction), i.e., the components of a mixture is confined in a regular simplex and, if linear constraints are imposed on these components, in a polytope within that simplex. An introduction to the theory, model building, and the construction of the experimental design will now be discussed.

Let $x_i,\ i = 1, 2 \ldots q$ denote the proportions of a q-component mixture, then $0 \le x_i \le 1$ and $\sum_{i=1}^{q} x_i = 1$. It then follows that the mixture variable $\boldsymbol{x} = \left(x_1, x_2, \ldots, x_q\right)$ lies in the regular $(q-1)$-dimensional simplex S and that the domain D_x of $\boldsymbol{x}$ is a subset of, or coincides with that simplex. Now let $x_i,\ i = 1, 2$ denote the *n*- and iso- paraffin components in the *n*/iso- paraffin mixture experiment.

The effect of the carbon number fractions on the response is also of interest. Let $z_i,\ i = 1, 2 \ldots r,\ r = 10$, denote the proportions of the carbon number components, then $0 < a_i \le z_i \le b_i < 1$ and $\sum_{i=1}^{r} z_i = 1$. The a_i and b_i are the lower and upper limits, respectively, of the C_9–C_{18} *n*- and

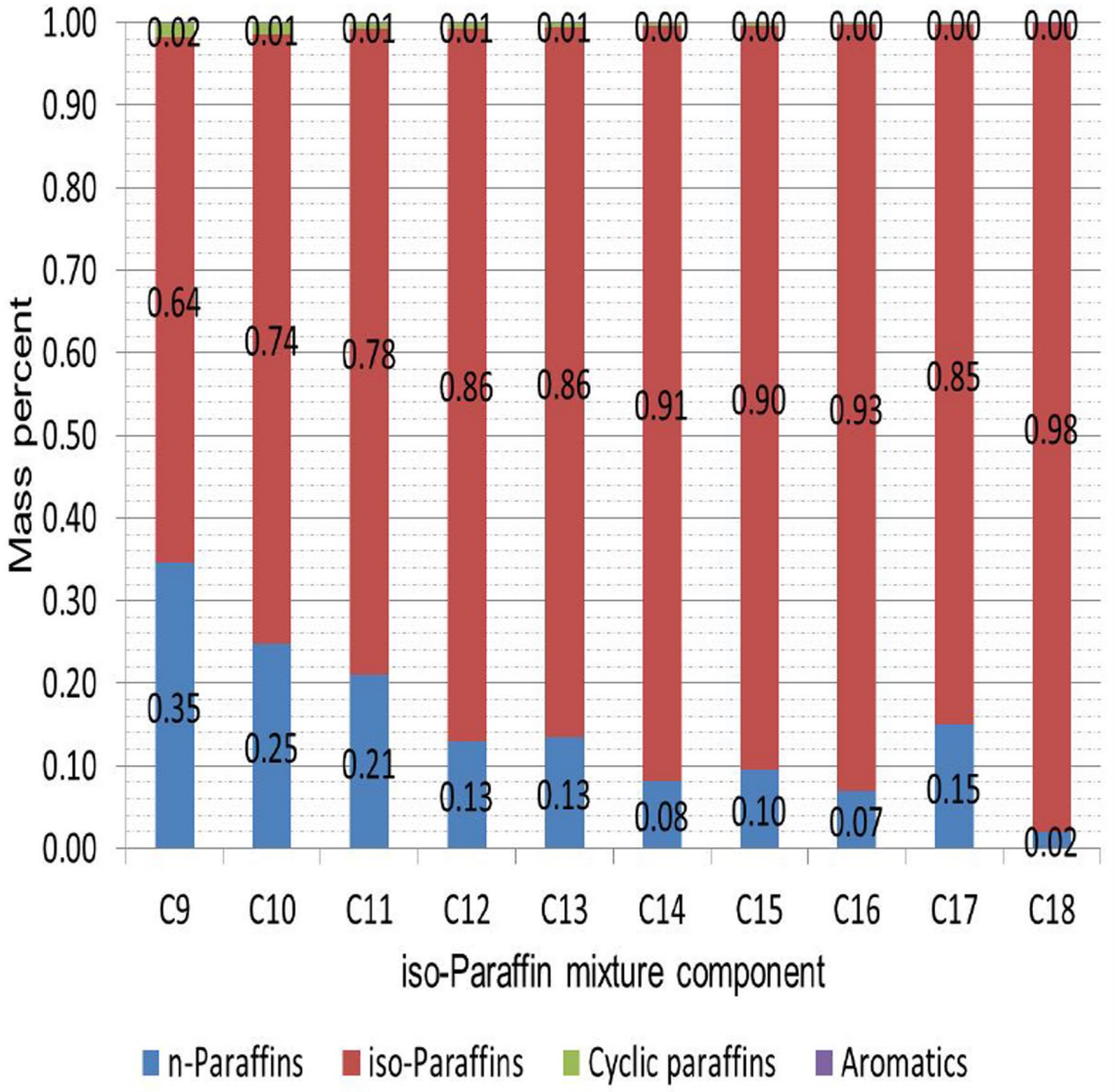

Fig. 2 Compositional graph of iso-paraffin GC×GC results

iso-paraffin carbon numbers. Therefore, the domain D_z of the mixture variable $\boldsymbol{z} = (z_1, z_2, \ldots, z_r)$ is a constrained polyhedron within the regular $(r-1)$-dimensional simplex S.

Now consider an experiment in which the response of a continuous variable (e.g. freeze point), y, to the mixtures $\boldsymbol{x}$ and $\boldsymbol{z}$ is of interest. The required response surface model can be formulated broadly as

$$y = F(\boldsymbol{x}, \boldsymbol{z}) + \varepsilon, \tag{1}$$

where y denotes the response of interest, $F(\cdot)$ is a deterministic function of the vectors of proportions $\boldsymbol{x} = (x_1, x_2)$ and $\boldsymbol{z} = (z_1, z_2, \ldots, z_{10})$, and ε represents an independent error term with mean 0 and constant variance σ^2. Scheffè polynomials are used extensively to model the response of such mixture experiments [12, 13]. The components of the final model is constructed from the following quadratic Scheffè polynomials

$$f(\boldsymbol{x}) = \sum_{i=1}^{2} \beta_i x_i + \beta_{12} x_1 x_2 \tag{2}$$

and

$$g(\boldsymbol{z}) = \sum_{i=1}^{r} \gamma_i z_i + \sum_{i=1}^{r-1} \sum_{j=i+1}^{r} \gamma_{ij} z_i z_j \tag{3}$$

relating to the i:n mass ratios and carbon number mixtures, respectively, and $\beta_i, \beta_{12}, \gamma_i, \gamma_{ij}$ are appropriately indexed unknown parameters. Note that setting the interaction

parameters equal to zero, i.e., $\beta_{12} = 0,\ \gamma_{ij} = 0$, yields the linear Scheffè polynomials. The global model which incorporates the *i*:*n* mass ratios and carbon number mixtures can be formulated as a mixture-by-mixture model and is specified as the product of the appropriate Scheffè polynomials. However, since the model in the carbon number mixtures is high dimensional, it was decided that only the linear effect of the carbon number mixtures on the response will be studied. The mixture-by-mixture model is specified as

$$F(\boldsymbol{x},z) = f(x)g(z) = \sum_{i=1}^{2}\sum_{j=1}^{10}\delta_{ij}x_i z_j + \sum_{j=1}^{10}\delta_{12j}x_1x_2z_j, \tag{4}$$

where $\delta_{ij} = \beta_i\gamma_j$ and $\delta_{12j} = \beta_{12}\gamma_j$. Model (4) has 30 parameters to estimate.

Optimal design of experiments

More generally, observations from an experiment can be modelled as

$$y_u = \boldsymbol{h}^T(\boldsymbol{x_u}, z_u)\boldsymbol{\delta} + \varepsilon_u,\ u = 1,\ldots,n,$$

where y_u denotes the response at the mixture setting $(\boldsymbol{x_u}, z_u)$., $\boldsymbol{h}^T(\boldsymbol{x_u}, z_u)\boldsymbol{\delta}$ represents model (4) with $\boldsymbol{h}^T(\boldsymbol{x_u}, z_u)$ a vector with appropriate monomials in the elements of $(\boldsymbol{x_u}, z_u)$ and $\boldsymbol{\delta}$ the vector of unknown parameters. The predicted values are obtained from $\hat{y}_u = \boldsymbol{h}^T(\boldsymbol{x_u}, z_u)\hat{\boldsymbol{\delta}}$. Therefore, an experimental design needs to be specified for estimating the parameters $(\hat{\boldsymbol{\delta}})$ in model (4) most precisely, and yield minimum variance of prediction $(\hat{y}_u)$. Coetzer and Haines [14] discussed how experimental designs for mixture-by-mixture models and mixture-by-process variable models can be constructed and built up in blocks. In the case of the i:n mass ratios the domain D_x is unconstrained and coincides with the one-dimensional simplex; therefore, a simplex-centroid design consisting of the pure component proportions and the 50:50 binary blend may suffice [12].

However, in the case of the carbon number mixtures, the domain D_z is constrained and the usual simplex-lattice or simplex-centroid designs are no longer applicable, and an experimental design needs to be specified using optimal experimental design theory given the postulated response surface model. Atkinson et al. [13] and the recent paper by Goos et al. [15] provided excellent overviews of optimal experimental design for mixture experiments. In practice, interest centres on exact *n*-point designs which allocate observations to the mixture variables $(\boldsymbol{x_u}, z_u),\ u = 1,\ldots,n$. Optimality criteria are appropriate functions of the information matrix for the unknown parameters $\boldsymbol{\delta}$ at the design ω_n, that is $\boldsymbol{M}(\omega_n) = \sum_{u=1}^{n}\boldsymbol{h}(\boldsymbol{x_u}, z_u)\boldsymbol{h}^T(\boldsymbol{x_u}, z_u)$. Goos et al. [15] recommended applying the *I*-optimality criterion, which are designs minimising the integrated variance of the predicted responses over the domain of the mixture settings, for constraint mixture experiments. Specifically, the *I*-optimality criterion is

$$\psi_{\boldsymbol{I}}(\omega_n) = \int_D \boldsymbol{h}^T(\boldsymbol{x},z)\boldsymbol{M}^{-1}\boldsymbol{h}(\boldsymbol{x},z)\mathrm{d}\boldsymbol{x}\mathrm{d}z = \mathrm{trace}\left[\boldsymbol{M}^{-1}\boldsymbol{L}\right], \tag{5}$$

where $\boldsymbol{L} = \int_D \boldsymbol{h}(\boldsymbol{x},z)\boldsymbol{h}^T(\boldsymbol{x},z)\mathrm{d}\boldsymbol{x}\mathrm{d}z$, the moment matrix which, strictly, should be divided by $\int_D \mathrm{d}\boldsymbol{x}\mathrm{d}z$. Due to the domain $D = D_x \times D_z$ being a constrained mixture space the integral in (5) cannot be calculated explicitly and must be approximated empirically over a fine grid of points over the domain D. The *I*-optimal design specifies the *n*-point design which minimises criterion (5) [13]. The domain D is of dimension 20, and consequently the problem of constructing exact *I*-optimal designs for such mixture experiments with observations fitted to a Scheffè polynomial model and with design points lying in a convex polytope defined by linear constraints is not straightforward. Generating exact optimal designs requires specifying a large candidate set of size N, $N >> n$, over the domain D from which the algorithm selects the *n*-points that minimizes the *I*-optimality criterion [13]. Specifically, the search for *I*-optimal designs for estimating model (4) turned out to be fruitless since a feasible candidate set could not be found over the domain D using various algorithms; the domain D being too constrained. To simplify the problem, it was decided to omit one of the carbon number components and consider the carbon number variables as independent process variables, subject to constraints. Therefore, C_{18} was omitted and only C_9–C_{17} were used in the design construction represented by $z_i,\ i = 1,2,\ldots,9$, subject to the constraint

$$0.6 \le \sum_{i=1}^{9} z_i \le 1 \tag{6}$$

Constraint (6) specifies that $0 \le z_{10} < 0.4$ for C_{18}. Consequently, model (4) needs to be re-written as a mixture-by-process variable response surface model

$$F_2(\boldsymbol{x},z) = \delta_1x_1 + \delta_2x_2 + \sum_{i=1}^{2}\sum_{j=1}^{9}\delta_{ij}x_iz_j + \sum_{j=1}^{9}\delta_{12j}x_1x_2z_j \tag{7}$$

See Cornell [12] for a detailed explanation on how to construct mixture-by-process variable models. The focus now centres on specifying an *I*-optimal design for minimising the variance of prediction from fitting observations to model (7). Model (7) has 29 parameters to estimate but is much more tractable since the domain is now specified in terms of mixture and independent process variables, which are now nine variables instead of 10.

The Design-Expert® software was used to construct the candidate set as follows [16]. First an experimental design was constructed in the *i*:*n* mass ratios over domain D_x for estimating the quadratic Scheffè polynomial (2). The candidate set consisted of the two vertices, the centre point and interior points. Second an experimental design was constructed in the carbon number components C_9–C_{17} subject to constraint (6) over domain D_z for estimating the linear Scheffè polynomial. In addition to the vertices, the candidate set was augmented with the centre point and blends on the component axes. By crossing these two designs, the Design-Expert® software then generates a candidate set consisting of 3605 points in total.

The *I*-optimality criterion is then applied over the candidate set to select the optimal 50 points from the 3605 points which minimizes the variance of prediction for model (7). The software uses the point-exchange algorithm [13]. The 50 points were constituted as follows: 29 unique points for model estimation, 12 additional points for lack of fit testing and 9 replications. The replications are important for estimating experimental error. The final design is depicted in Table 1 and is optimal for studying jet fuel properties as a function of *n*- and iso-paraffin components and carbon number distribution. The specified set of mixtures was prepared and the freeze point and viscosity were measured for each mixture. The data were fitted to the response surface model (7). The pure error of the experimental data was determined using replicate blends in the design and was found to be 0.3 °C for freeze point and 2.6×10^{-3} cSt for viscosity.

Rationalisation of viscosity measurement temperature

ASTM D1655-16c [10] states that jet fuel may potentially exceed the maximum allowable 12 cSt viscosity specified by APU manufacturers as the fuel approaches the freeze point specification limit (− 40 °C for Jet A or − 47 °C for Jet A-1), when the viscosity at − 20 °C exceeds 5.5 cSt for Jet A or 4.5 cSt for Jet A-1. Since it is problematic to measure viscosity at extremely low temperatures such as − 47 °C, the initial viscosity measurement temperature was chosen as − 20 °C. During analyses of the sample population generated by the Design-Expert® software, it became apparent that it would not be possible to measure the viscosities at − 20 °C for a large portion of the sample population; viscosity measurements were consequently conducted at 20 °C.

ASTM D341 can be employed to establish the kinematic viscosity of liquid hydrocarbons within a limited range, provided that viscosity values at two temperatures are known [17]. This method was employed to attain a proposed maximum viscosity value of 1.8 cSt at 20 °C, by use of the 12 and 4.5 cSt viscosity limits discussed previously.

Statistical models and discussion

Model for viscosity

The viscosity data are given in Table 1. Model (7) was fitted on the data using the Design-Expert® software [16]. The estimated model obtained for viscosity ($\hat{y}_1$) is:

$$\begin{aligned}\hat{y}_1 = {} & 5.39n\text{ - paraffin } + 4.39\text{ iso - paraffin } + 0.13n\text{ - paraffin} \cdot \text{iso - paraffin } - 5.69n\text{ - paraffin} \cdot C_9 - 4.95n\text{ - paraffin} \cdot C_{10} - 4.62 \\ & n\text{ - paraffin} \cdot C_{11} - 3.44n\text{ - paraffin} \cdot C_{12} - 2.68n\text{ - paraffin} \cdot C_{13} - 1.81n\text{ - paraffin} \cdot C_{14} - 2.21n\text{ - paraffin.}C_{15} - 1.51n\text{ - paraffin} \cdot C_{16} \\ & - 0.71n\text{ - paraffin} \cdot C_{17} - 4.16\text{ iso - paraffin} \cdot C_9 - 3.98\text{ iso - paraffin} \cdot C_{10} - 3.30\text{ iso - paraffin} \cdot C_{11} - 2.47\text{ iso - paraffin} \cdot C_{12} - 1.69 \\ & \text{iso - paraffin} \cdot C_{13} - 2.12\text{ iso - paraffin} \cdot C_{14} - 1.35\text{ iso - paraffin} \cdot C_{15} - 0.70\text{ iso - paraffin} \cdot C_{16} - 0.09\text{ iso - paraffin} \cdot C_{17} + 2.34 \\ & n\text{ - paraffin} \cdot \text{iso - paraffin} \cdot C_{11} - 3.29n\text{ - paraffin} \cdot \text{iso - paraffin} \cdot C_{17}\end{aligned} \tag{8}$$

The variable names in model (8) represent the proportion of the specific component in the mixture. The model has 22 parameters which are all significant at or below the 10% significance level, i.e., there exists at least 90% confidence that the effect of the variable on the viscosity is true. Terms in Eq. (8) of the form *.* denote second-order interactions between two components and terms of the form *.*.* denote third-order interactions. The standard error of the model is 0.2 cSt, which is very small compared to the mean viscosity of 2.5 cSt. The model has a $R^2 = 0.96$, therefore, 96% of the variability is explained by the model. The adjusted $R^2 = 0.94$ and predicted $R^2 = 0.84$. The adjusted R^2 penalises the normal R^2 if non-significant parameters are included in the model, which in this case shows that the correct variables and effects have been included in the model to explain

Table 1 Optimal experimental design in *n*- and iso- paraffin components and carbon number distribution

Run	Mixture components (mass%)		Numeric factors (mass%)										Blend properties (responses)	
	iso-Paraffin	*n*-Paraffin	C_9	C_{10}	C_{11}	C_{12}	C_{13}	C_{14}	C_{15}	C_{16}	C_{17}	C_{18}	Freeze point (°C)	Viscosity at 20 °C (cSt)
1	0.50	0.50	0.10	0.10	0.10	0.10	0.10	0.10	0.10	0.10	0.10	0.10	− 10.3	2.4
2	1.00	0.00	0.00	0.00	0.00	0.00	0.20	0.00	0.00	0.40	0.40	0.00	− 37.9	4.0
3	0.50	0.50	0.40	0.20	0.00	0.00	0.40	0.00	0.00	0.00	0.00	0.00	− 33.8	1.4
4	0.00	1.00	0.00	0.00	0.40	0.00	0.00	0.00	0.00	0.20	0.40	0.00	8.1	3.0
5	0.50	0.50	0.00	0.00	0.40	0.00	0.20	0.00	0.00	0.00	0.40	0.00	− 2.9	2.6
6	0.00	1.00	0.00	0.00	0.00	0.00	0.00	0.40	0.00	0.20	0.00	0.40	14.4	4.5
7	0.50	0.50	0.40	0.00	0.00	0.00	0.00	0.00	0.20	0.00	0.40	0.00	− 5.1	2.2
8	1.00	0.00	0.00	0.40	0.00	0.20	0.00	0.00	0.00	0.00	0.40	0.00	− 43.0	2.1
9	0.50	0.50	0.20	0.00	0.40	0.40	0.00	0.00	0.00	0.00	0.00	0.00	− 34.2	1.5
10	0.50	0.50	0.00	0.00	0.00	0.40	0.20	0.00	0.00	0.40	0.00	0.00	− 4.2	2.7
11	0.50	0.50	0.00	0.00	0.00	0.00	0.40	0.20	0.40	0.00	0.00	0.00	− 12.7	2.9
12	1.00	0.00	0.00	0.00	0.00	0.40	0.00	0.00	0.00	0.00	0.20	0.40	− 37.3	3.5
13	1.00	0.00	0.00	0.00	0.20	0.40	0.00	0.00	0.40	0.00	0.00	0.00	− 56.6	2.2
14	0.00	1.00	0.00	0.20	0.00	0.00	0.00	0.00	0.40	0.00	0.00	0.40	11.8	3.5
15	0.50	0.50	0.00	0.00	0.00	0.40	0.00	0.20	0.00	0.00	0.40	0.00	− 2.6	3.0
16	1.00	0.00	0.00	0.00	0.00	0.40	0.20	0.00	0.00	0.40	0.00	0.00	− 52.3	2.6
17	0.75	0.25	0.00	0.40	0.20	0.00	0.40	0.00	0.00	0.00	0.00	0.00	− 42.5	1.6
18	0.00	1.00	0.40	0.00	0.00	0.00	0.00	0.40	0.20	0.00	0.00	0.00	− 9.7	1.9
19	0.50	0.50	0.20	0.00	0.00	0.00	0.00	0.40	0.00	0.40	0.00	0.00	− 9.9	2.5
20	1.00	0.00	0.40	0.00	0.00	0.00	0.00	0.00	0.00	0.40	0.00	0.20	− 44.0	2.1
21	0.50	0.50	0.00	0.20	0.00	0.40	0.00	0.00	0.00	0.00	0.00	0.40	0.5	2.6
22	1.00	0.00	0.20	0.00	0.00	0.00	0.00	0.00	0.40	0.00	0.40	0.00	− 42.6	2.8
23	0.50	0.50	0.00	0.40	0.20	0.00	0.00	0.40	0.00	0.00	0.00	0.00	− 19.6	1.7
24	0.00	1.00	0.40	0.00	0.20	0.00	0.00	0.00	0.00	0.00	0.00	0.40	6.6	2.1
25	0.50	0.50	0.00	0.40	0.00	0.00	0.00	0.00	0.40	0.20	0.00	0.00	− 12.4	2.2
26	0.50	0.50	0.20	0.00	0.40	0.00	0.00	0.00	0.40	0.00	0.00	0.00	− 19.0	1.8
27	0.50	0.50	0.00	0.00	0.00	0.00	0.20	0.40	0.00	0.00	0.00	0.40	2.3	3.8
28	1.00	0.00	0.20	0.00	0.00	0.00	0.40	0.40	0.00	0.00	0.00	0.00	− 53.6	2.0
29	0.00	1.00	0.00	0.00	0.00	0.40	0.00	0.00	0.40	0.20	0.00	0.00	0.4	2.9
30	1.00	0.00	0.40	0.20	0.00	0.40	0.00	0.00	0.00	0.00	0.00	0.00	BDL	1.2
31	0.50	0.50	0.00	0.00	0.20	0.00	0.00	0.00	0.00	0.40	0.00	0.40	4.1	4.0
32	0.00	1.00	0.00	0.40	0.00	0.40	0.00	0.00	0.00	0.00	0.20	0.00	− 5.1	1.9
33	0.00	1.00	0.00	0.40	0.00	0.40	0.00	0.00	0.00	0.00	0.20	0.00	− 5.2	1.9
34	0.50	0.50	0.10	0.10	0.10	0.10	0.10	0.10	0.10	0.10	0.10	0.10	− 10.4	2.4
35	0.50	0.50	0.10	0.10	0.10	0.10	0.10	0.10	0.10	0.10	0.10	0.10	− 10.4	2.4
36	0.50	0.50	0.00	0.00	0.00	0.00	0.40	0.20	0.40	0.00	0.00	0.00	− 12.6	2.9
37	0.50	0.50	0.40	0.00	0.00	0.00	0.00	0.00	0.20	0.00	0.40	0.00	− 5.3	2.2
38	0.00	1.00	0.00	0.40	0.00	0.00	0.20	0.00	0.00	0.40	0.00	0.00	2.7	2.2
39	0.00	1.00	0.00	0.40	0.00	0.00	0.20	0.00	0.00	0.40	0.00	0.00	2.4	2.2
40	0.50	0.50	0.00	0.00	0.40	0.00	0.20	0.00	0.00	0.00	0.40	0.00	− 3.7	2.6
41	0.00	1.00	0.20	0.00	0.00	0.40	0.40	0.00	0.00	0.00	0.00	0.00	− 17.5	1.8
42	1.00	0.00	0.20	0.00	0.00	0.00	0.00	0.40	0.00	0.00	0.40	0.00	− 45.2	2.6
43	1.00	0.00	0.00	0.00	0.40	0.00	0.40	0.00	0.00	0.20	0.00	0.00	− 62.5	2.1
44	0.00	1.00	0.00	0.00	0.40	0.00	0.40	0.20	0.00	0.00	0.00	0.00	− 14.7	2.1
45	0.50	0.50	0.00	0.00	0.20	0.00	0.00	0.00	0.00	0.40	0.00	0.40	4.2	4.0
46	1.00	0.00	0.00	0.00	0.40	0.00	0.00	0.40	0.00	0.20	0.00	0.00	− 55.6	2.2
47	1.00	0.00	0.00	0.00	0.00	0.00	0.20	0.00	0.40	0.40	0.00	0.00	− 43.5	3.5

Table 1 (continued)

Run	Mixture components (mass%)		Numeric factors (mass%)										Blend properties (responses)	
	iso-Paraffin	*n*-Paraffin	C_9	C_{10}	C_{11}	C_{12}	C_{13}	C_{14}	C_{15}	C_{16}	C_{17}	C_{18}	Freeze point (°C)	Viscosity at 20 °C (cSt)
48	0.50	0.50	0.40	0.20	0.00	0.00	0.40	0.00	0.00	0.00	0.00	0.00	−34.6	1.4
49	1.00	0.00	0.00	0.40	0.00	0.00	0.00	0.00	0.20	0.00	0.00	0.40	−40.4	2.5
50	0.00	1.00	0.00	0.00	0.00	0.00	0.40	0.00	0.00	0.00	0.40	0.20	13.9	4.0

BDL below detection limit

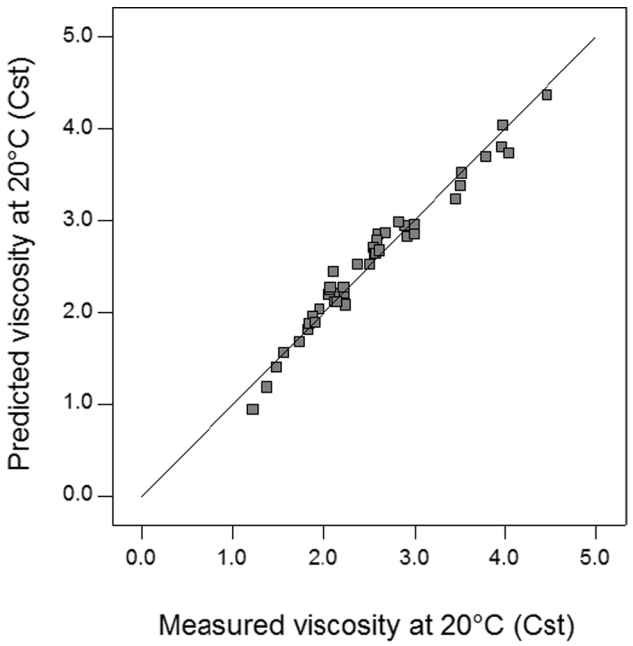

Fig. 3 Parity plot of the response surface model for viscosity

the variability in viscosity, and the model is not over parametrized [12]. The predicted R^2 is a leave-one-out cross-validation statistic, and indicates the amount of variability explained for new points which were not used in fitting the model. In this case, 84% of new points were predicted correctly, which is very good [12]. Figure 3 depicts the parity plot for the response surface model (8) for viscosity. Therefore, model (8) can be used to predict viscosity as a function of the *n*- and iso-paraffin components and carbon number distribution, within the experimental range specified.

Interpreting the effect of the mixture components on the viscosity can best be done by generating predicted contours as a function of changes in the mixture components using model (8). Figure 4 depicts predicted contours of viscosity for two different compositions of the i:n mass ratio. Figure 4a depicts the predicted contours as a function of changing C_{11} and C_{12} for *n*-paraffin = 0.16 and iso-paraffin = 0.84. It is clear that the viscosity increases with a decrease in the amounts of C_{11} and C_{12} in the blend. Figure 4b depicts the predicted contours as a function of changing C_{11} and C_{12} for *n*-paraffin = 0.95 and iso-paraffin = 0.05. The effect of the amounts of C_{11} and C_{12} in the blend is marginally greater for higher proportions of *n*-paraffin compared to iso-paraffin in the blend. The graphs are similar in appearance since the viscosity differences between the *n*- and iso-paraffin mixture components are marginal in the C_9–C_{16} carbon number range. Since the C_{17} and C_{18} *n*-paraffin mixture components were solid at 20 °C, their viscosities could not be measured. However, it is obvious that larger quantities of these components would have a negative impact on the viscosity of jet fuel. Therefore, the carbon number distribution of the jet fuel blend has a significant effect on the viscosity of the blend.

Model for freeze point

The freeze point data are provided in Table 1. Model (7) were fitted on the data using the Design-Expert® software [16]. The estimated model obtained for freeze point ($\hat{y}_2$) is:

$$\begin{aligned}\hat{y}_2 =& 35.90n\text{ - paraffin} - 21.77\text{ iso - paraffin} + 66.43n\text{ - paraffin} \cdot \text{iso - paraffin} - 49.87n\text{ - paraffin} \cdot C_9 - 45.87n \\ &\text{- paraffin} \cdot C_{10} - 53.71n\text{ - paraffin} \cdot C_{11} - 53.17\quad n\text{ - paraffin} \cdot C_{12} - 51.16n\text{ - paraffin} \cdot C_{13} - 46.67n \\ &\text{- paraffin} \cdot C_{14} - 32.17n\text{ - paraffin} \cdot C_{15} - 13.19n\text{ - paraffin} \cdot C_{16} - 6.64n\text{ - paraffin} \cdot C_{17} \\ &- 42.56\text{ iso - paraffin} \cdot C_9 - 32.23\text{iso - paraffin} \cdot C_{10} - 55.83\text{ iso - paraffin} \cdot C_{11} - 36.71\text{ iso - paraffin} \\ &\cdot C_{12} - 38.87\text{ iso - paraffin} \cdot C_{13} - 23.04\text{ iso - paraffin} \cdot C_{14} - 21.43 \\ &\text{iso - paraffin} \cdot C_{15} - 15.30\text{ iso - paraffin} \cdot C_{16} - 7.70\text{ iso - paraffin} \cdot C_{17} - 96.40n\text{ - paraffin} \cdot \text{iso - paraffin} \cdot C_9 \\ &- 50.69n\text{ - paraffin} \cdot \text{iso - paraffin} \cdot C_{10} + 59.44n\text{ - paraffin} \cdot \text{iso - paraffin} \cdot C_{17}\end{aligned} \tag{9}$$

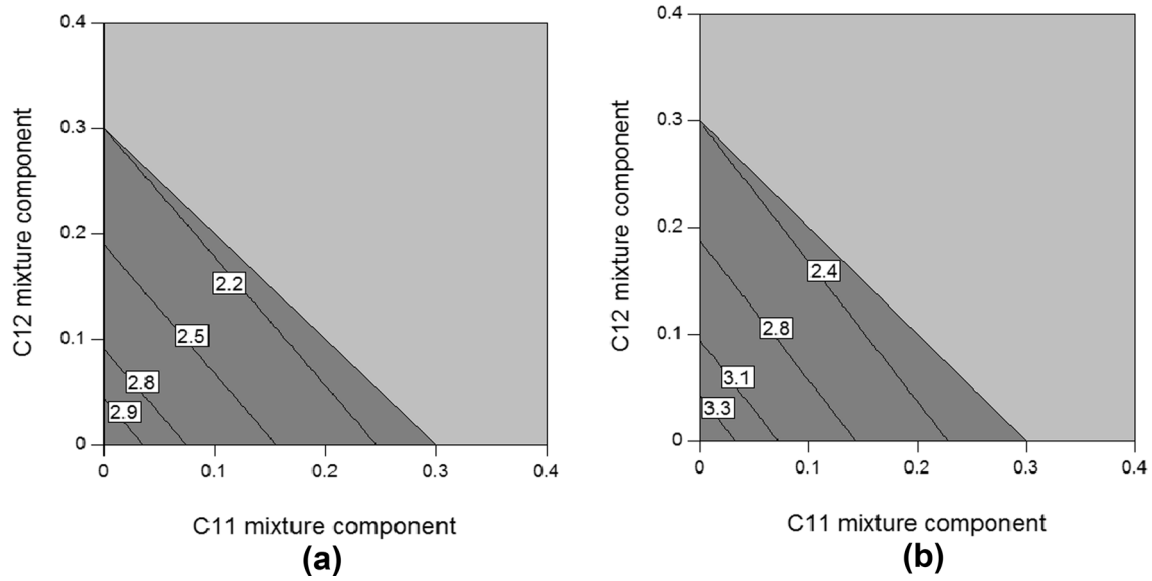

Fig. 4 Predicted contours of viscosity as a function of changes in the mixture variables. **a** Predictions as a function of changing C_{11} and C_{12} for *n*-paraffin = 0.16 and iso-paraffin = 0.84; **b** predictions as a function of changing C_{11} and C_{12} for *n*-paraffin = 0.95 and iso-paraffin = 0.05

The variable names in model (9) represent the proportion of the specific component in the mixture. Terms in Eq. (9) of the form *.* denote second-order interactions between two components and terms of the form *.*.* denote third-order interactions. The model exhibited a R^2 value of 0.99, therefore 99% of the variation in the freeze point data was accounted for by the model. The adjusted R^2 value was 0.98. The adjusted R^2 penalises the normal R^2 if non-significant parameters are included in the model, which in this case shows that the correct variables were included in the model to explain the variability in freeze point, and the model did not contain unnecessary parameters. The cross-validated R^2 value indicates that the model accurately predicted 96% of the freeze points for new mixtures. In addition, the fact that all three R^2 statistics are very similar in value confirms that this is an excellent model for freeze point. All model parameters were at or below the 10% significance level; none of the parameters could thus be excluded from the model. The freeze point of jet fuel must be reported accurately to ± 1.0 °C [10]. The standard error of the model was 2.7 °C, which is 1.7 °C wider than the 1.0 °C reporting value stipulated by ASTM D1655 [10]. When considering the complexity of the mixture design, this difference is deemed to be sufficiently small and the model was thus still considered fit for use.

Figure 5 depicts the scatter plot obtained from Design-Expert® for comparison of the predicted- and measured freeze points of model (9). The majority of the observations were scattered close to the diagonal line. The model (9) can, therefore, be used to predict freeze point as a function of the *i*:*n* mass ratio and carbon number distribution.

The effect of the *i*:*n* mass ratio and carbon number distribution on freeze point was studied by generating predicted contours as a function of changes in the mixture components. Figure 6 depicts predicted contours of freeze point for different compositions of the *i*:*n* mass ratio. Figure 6a depicts the predicted contours as a function

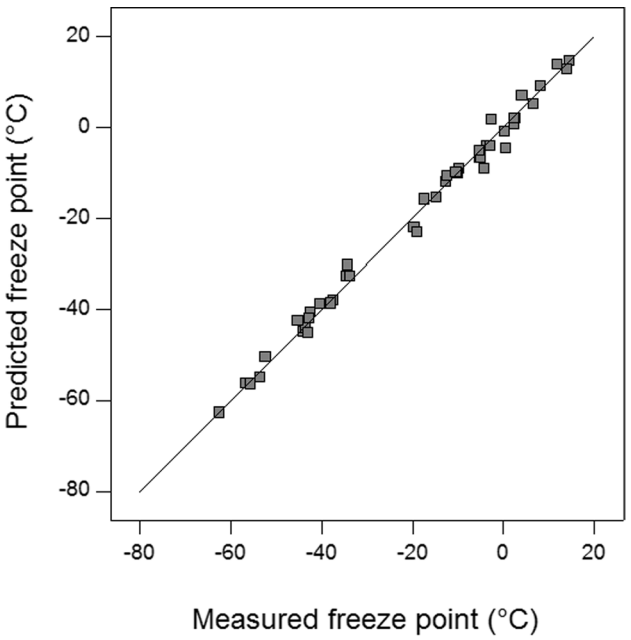

Fig. 5 Parity plot of the response surface model for freeze point

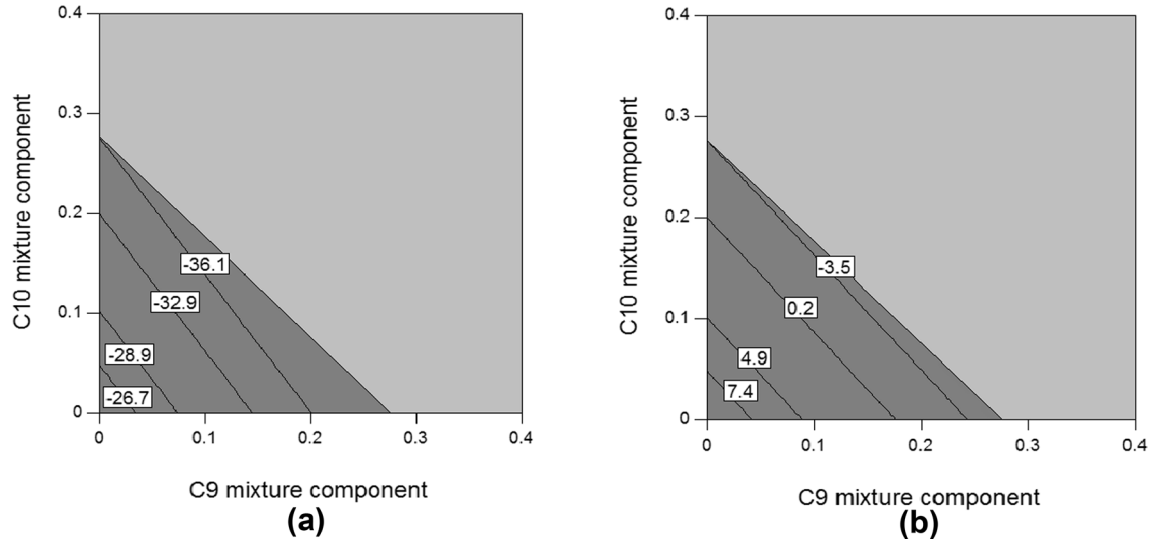

Fig. 6 Predicted contours of freeze point as a function of changes in the mixture variables. **a** Predictions as a function of changing C_9 and C_{10} for *n*-paraffin = 0.16 and iso-paraffin = 0.84; **b** predictions as a function of changing C_9 and C_{10} for *n*-paraffin = 0.95 and iso-paraffin = 0.05

of changing C_9 and C_{10} for *n*-paraffin = 0.16 and iso-paraffin = 0.84. It can be observed that the freeze point is very low and increased significantly as the amounts of C_9 and C_{10} components in the mixture decreased. Figure 6b depicts the predicted contours as a function of changing C_9 and C_{10} for *n*-paraffin = 0.95 and iso-paraffin = 0.05. The freeze point also increased significantly as the amounts of C_9 and C_{10} components decreased. Affens et al. [18] studied the effect of composition on the freeze point of model hydrocarbon fuels. The authors found that when a high freeze point hydrocarbon is dissolved in a suitable low freeze point solute, and an ideal solution is formed, this ideal solution will possess a freeze point which is equivalent to that of the solute [18]. It is believed that the C_9 and C_{10} mixture components in this study serve as solvents for the longer carbon chain length mixture components, thereby decreasing the freeze point of the mixture as the relative proportions of the C_9 and C_{10} components increase within the mixture. When comparing Fig. 6a, b, it can be observed that mixtures which contained higher concentrations of *n*-paraffins exhibited higher freeze points. Therefore, the *i*:*n* mass ratio in the jet fuel mixture has a significant effect on the freeze point of the blend. Furthermore, the effect of the carbon number distribution on the freeze point is dependent on the *i*:*n* mass ratio of the jet fuel blend.

Validation

It is required to validate the models developed for new blends. Therefore, additional jet fuel blends were prepared for which the freeze point and viscosity properties were determined.

Coetzer et al. [19] applied dual response surface optimization for optimising the variable conditions for a coal gasification process, and discussed a number of approaches for multiple response optimizations. The Design-Expert® software [16] applies the desirability function approach of Derringer and Suich [20] for multiple response optimizations. Two properties of jet fuel blends were measured in this study, i.e., viscosity (y_1) and freeze point (y_2), as functions of the i:n mass ratio and carbon number distribution. According to APU specifications the freeze point of Jet A-1 is required to be lower than −47 °C with minimum viscosity. Let the target for freeze point be $T_2 = \hat{y}_{2,\min}$, i.e., the minimum value of the predicted freeze point from the model. Now the predicted value is transformed to a new value d_2 through a desirability function, which can also be viewed as the degree of satisfaction in reaching the target. The degree of satisfaction of the experimenter with respect to the mean response is maximised when $\hat{y}_2 = T_2$ and decreases as $\hat{y}_2$ moves away from T_2. The experimenter does not accept any solution for which $\hat{y}_2 > \hat{y}_{2,\max}$, which in the case of freeze point is specified as $\hat{y}_{2,\max} = -47$ °C. Thus the satisfaction level with respect to the mean response can be modelled by a function which increases monotonically from 0, at $\hat{y}_2 = \hat{y}_{2,\max}$ to 1, at $\hat{y}_2 = T_2$. The desirability value of the mean response, which is denoted as d_2, is interpreted as the degree to which $\hat{y}_2$ satisfies the target on the mean and is a value between 0 and 1.

For the freeze point, the desirability function is

Table 2 Validation mixtures

Run	1	2	3	4	5	6	7	8	9
n-Paraffin	0.00	0.02	0.02	0.04	0.05	0.05	0.07	0.10	0.11
iso-Paraffin	1.00	0.98	0.98	0.96	0.95	0.95	0.93	0.90	0.89
C_9	0.14	0.21	0.04	0.04	0.04	0.29	0.15	0.06	0.13
C_{10}	0.33	0.21	0.25	0.04	0.20	0.24	0.17	0.04	0.01
C_{11}	0.09	0.06	0.01	0.39	0.05	0.01	0.22	0.27	0.34
C_{12}	0.04	0.03	0.13	0.04	0.35	0.18	0.13	0.03	0.35
C_{13}	0.04	0.07	0.12	0.03	0.07	0.00	0.04	0.39	0.01
C_{14}	0.05	0.12	0.26	0.39	0.08	0.13	0.08	0.03	0.01
C_{15}	0.04	0.17	0.18	0.03	0.21	0.02	0.05	0.04	0.01
C_{16}	0.11	0.02	0.00	0.01	0.00	0.06	0.04	0.10	0.01
C_{17}	0.02	0.03	0.00	0.01	0.00	0.05	0.05	0.02	0.01
C_{18}	0.15	0.08	0.00	0.02	0.00	0.02	0.05	0.02	0.10
Measured freeze point (°C)	−52.2	−50.0	−51.9	−51.6	−49.0	−46.3	−36.9	−42.7	−29.7
Measured viscosity at 20 °C (cSt)	1.8	1.8	1.9	1.9	1.9	1.5	1.7	2.0	1.7
Predicted freeze point (°C)	−50.0	−50.0	−50.0	−55.0	−50.0	−50.0	−50.0	−50.0	−50.0
Predicted viscosity at 20 °C (cSt)	1.8	1.8	1.8	1.8	1.8	1.4	1.7	2.2	1.8

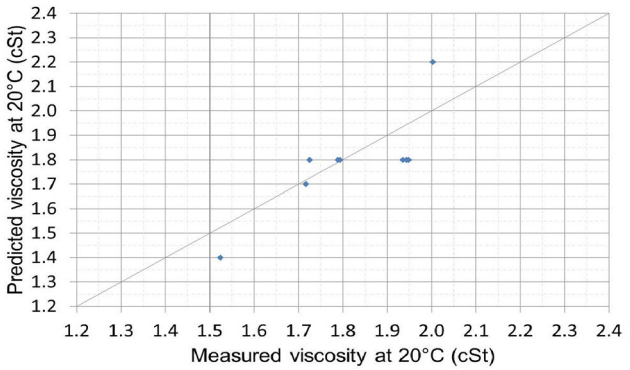

Fig. 7 Parity plot of viscosity for the validation mixtures

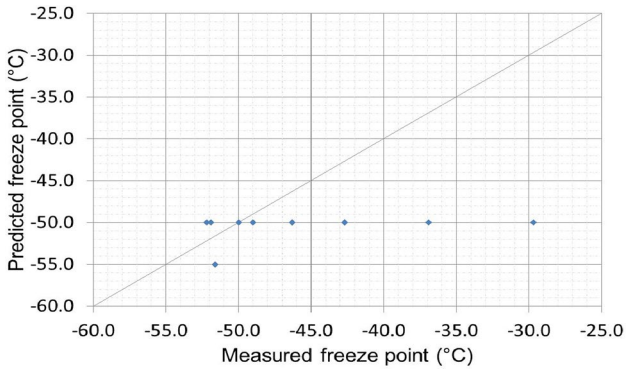

Fig. 8 Parity plot of freeze point for the validation mixtures

$$d_2 = \begin{cases} 1 & \text{if } \hat{y}_2 \le T_2 \\ \left[\frac{(\hat{y}_{2,\max} - \hat{y}_2)}{(\hat{y}_{2,\max} - T_2)}\right]^r & \text{if } T_2 < \hat{y}_2 \le \hat{y}_{2,\max} \\ 0 & \hat{y}_2 > \hat{y}_{2,\max} \end{cases}, \quad (10)$$

where r is the weight of the function. Therefore, d_2 approaches one as $\hat{y}_2$ approaches the target T_2, and equals one if $\hat{y}_2 = T_2$. The value of r can be chosen according to the experiments preference and how important it is to be closer to the target than further from it; if $r = 1$, then the desirability function is linear and indicates an average increase in satisfaction as the response approaches the target. Choosing $r > 1$ makes the function non-linear and results in placing more emphasis on being closer to the target value, and choosing $0 < r < 1$ makes it less important or more tolerable to be more remote from the target. See Coetzer et al. [19] for a more detailed discussion on desirability functions and optimization strategies.

The desirability function (d_1) for viscosity ($\hat{y}_1$) has the same form as d_2 in (10). Therefore, for viscosity, $T_1 = \hat{y}_{1,\min}$ and $\hat{y}_{1,\max}$ is equal to the maximum predicted value for viscosity. The overall desirability for the dual responses is specified as

$$\overline{d} = \left(d_1 \times d_2\right)^{0.5} \quad (11)$$

Therefore, if either of the individual desirability values is equal to zero, then the overall desirability is equal to zero. The optimization algorithm aims to find the optimal blends by forcing the individual desirability functions to be closer to one in order to maximise the overall desirability.

Nine validation mixtures were obtained by entering the desired responses into the numerical optimisation

function of the Design-Expert® software [16] and allowing it to suggest optimal solutions for meeting the specified response criteria by use of the overall desirability function $\bar{d}$. The results are depicted in Table 2. The differences between the measured- and predicted viscosity at 20 °C for all mixtures were negligible. It can also be observed that the differences between the measured- and predicted freeze point results varied considerably. Certain predicted freeze point results were fairly accurate, whereas others were decidedly inaccurate, as indicated by the freeze point results of optimal mixture numbers two and nine. Accuracy of the freeze point prediction results also appeared to decrease significantly when *n*-paraffin > 0.05.

Figure 7 depicts the parity plot of viscosity for the validation mixtures. At first glance it appears as if some observations were scattered far from the diagonal line at 45°; however, the scale of the *x*- and *y*-axes should be taken into consideration; both axes are scaled from 1.2 to 2.4 cSt, which is quite narrow and might adversely affect deductions made when studying the graph without taking note of this. Furthermore, all validation blends yielded errors which are within the model error of 0.2 cSt. The viscosity model can thus be used with confidence to predict viscosity as a function of the *i*:*n* mass ratio and carbon number distribution.

Figure 8 depicts the parity plot of freeze point for the validation mixtures. The three observations to the right on the *x*-axis (the measured freeze point axis) yielded severe validation errors. The most notable outlier was validation mixture number nine, which exhibited a predicted freeze point of − 50.0 °C, compared to a measured freeze point of − 29.7 °C. Four validation mixtures in Table 2 yielded validations errors which were within the model error of 2.7 °C. The freeze point model must thus be used with caution.

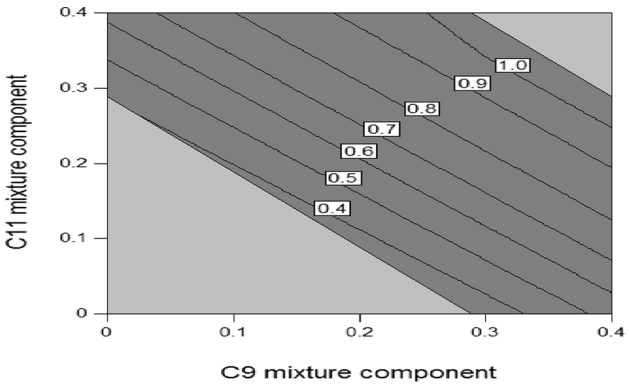

Fig. 9 Overall desirability as a function of changes in C_9 and C_{11} for *n*-paraffin = 0, iso-paraffin = 1, C_{12} = 0.33 and the other carbon number approximately zero

Optimization studies

After development of response surface models for predicting freeze point and viscosity, optimization studies can be conducted for specifying the optimum jet fuel blends to satisfy specific targets for the freeze point and viscosity of the blend. This is important for recommendations on suitable jet fuel blends for the industry. However, as highlighted with the validation results in "Validation", it is always advisable to validate the optimum blends obtained by the numerical optimization algorithm.

Table 3 Optimum blends for minimizing freeze point and viscosity simultaneously

Run	1	2	3	4	5	6	7	8	9	10
n-Paraffin	0	0	0	0	0	0	0	0	0	0
iso-Paraffin	1	1	1	1	1	1	1	1	1	1
C_9	0.30	0.22	0.22	0.30	0.24	0.05	0.32	0.31	0.30	0.32
C_{10}	0.02	0.20	0.15	0.04	0.24	0.33	0.10	0.06	0.16	0.12
C_{11}	0.32	0.34	0.30	0.32	0.30	0.40	0.35	0.27	0.27	0.33
C_{12}	0.33	0.10	0.09	0.21	0.02	0.02	0.02	0.26	0.00	0.03
C_{13}	0.01	0.05	0.06	0.02	0.10	0.05	0.01	0.01	0.13	0.09
C_{14}	0.00	0.02	0.09	0.04	0.00	0.07	0.01	0.01	0.00	0.00
C_{15}	0.01	0.02	0.08	0.00	0.02	0.02	0.13	0.05	0.13	0.01
C_{16}	0.01	0.02	0.00	0.02	0.06	0.02	0.06	0.03	0.01	0.07
C_{17}	0.00	0.01	0.00	0.04	0.00	0.03	0.00	0.01	0.00	0.01
C_{18}	0.00	0.02	0.01	0.01	0.02	0.01	0.00	− 0.01	0.00	0.02
Predicted freeze point (°C)	− 65.9	− 63.9	− 62.5	− 64.0	− 62.8	− 62.6	− 63.0	− 62.8	− 62.6	− 63.5
Predicted viscosity at 20 °C (cSt)	1.1	1.1	1.2	1.2	1.1	1.2	1.2	1.2	1.2	1.2
Desirability	1	1	1	1	1	1	1	1	1	1

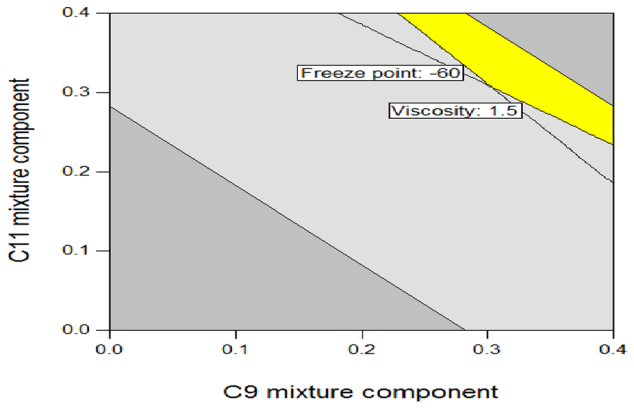

Fig. 10 Overlay plot of predicted contours for freeze point ($\hat{y}_2 \leq -60$ °C) and viscosity ($\hat{y}_1 \leq 1.5$ cSt). The yellow area indicates the blends which satisfy the requirements simultaneously for *n*-paraffin = 0, iso-paraffin = 1, $C_{12} = 0.33$ and the other carbon number approximately zero

Table 4 Final *i*:*n* ratio and carbon number distribution blend

n-Paraffin	0.05
iso-Paraffin	0.95
C_9	0.12
C_{10}	0.17
C_{11}	0.16
C_{12}	0.14
C_{13}	0.09
C_{14}	0.13
C_{15}	0.08
C_{16}	0.04
C_{17}	0.02
C_{18}	0.05
Measured freeze point (°C)	−47.1
Measured viscosity at 20 °C (cSt)	1.8
Measured viscosity at −20 °C (cSt)	4.3

The numerical optimisation function of the Design-Expert® software was applied to obtain optimal blends for minimising both freeze point and viscosity as predicted by their respective response surface models. Table 3 depicts 10 optimal blends which maximised the overall desirability $\bar{d}$ (Eq. 11) for minimising freeze point and viscosity simultaneously. All optimum blends specified a freeze point below −62 °C and viscosity smaller than 1.2 cSt. The iso-paraffin proportion in the blend must be maximised, the amount of C_9 in the blend should range from 22 to 32% and the amount of C_{11} should be between 27 and 40% for high overall desirability. The other carbon numbers did not contribute much to the optimum blends.

Figure 9 shows the contours of the overall desirability for changes in C_9 and C_{11} for *n*-paraffin = 0, iso-paraffin = 1. It is clear that the overall desirability increases with an increase in the C_9 and C_{11} fractions in the blend. Figure 10 displays an overlay plot of predicted contours for freeze point and viscosity for *n*-paraffin = 0, iso-paraffin = 1, $C_{12} = 0.33$ and the rest of the carbon numbers approximately equal to zero, except for C_{18} which makes up the remainder. The yellow area indicates the blends which satisfy the requirements of $\hat{y}_2 \leq -60$ °C for freeze point and $\hat{y}_1 \leq 1.5$ cSt for viscosity simultaneously. These optimization results provide for alternatives in selecting optimal blends which satisfy specified criteria for freeze point and viscosity simultaneously; however, it must be noted that volatility specifications, such as flash point, will regulate the quantities of C_9–C_{11} mixture components present in jet fuel blends [7].

Since the validation mixtures depicted in Table 2 were obtained by means of the numerical optimisation function of Design-Expert®, these mixtures can also be used for further optimisation studies. The before mentioned mixtures were thus used to determine the i:n ratio and carbon number distribution of Jet A-1 jet fuels with viscosities lower than 1.8 cSt at 20 °C and freeze points below −50 °C, respectively. For this purpose the average i:n mass ratio and carbon number distribution of the nine validation mixtures were calculated. The average *i*:*n* ratio and carbon number distribution were then used to prepare and analyse a final blend. Table 4 depicts the results of the final blend. The maximum allowable quantity of *n*-paraffins for mixtures that meet the specified criteria is thus 0.05. The measured viscosity of the mixture adhered to the self-proposed maximum viscosity limit of 1.8 cSt at 20 °C, as well as to the ASTM proposed maximum of 4.5 cSt at −20 °C. The measured freeze point of the mixture did not meet the specified −50 °C target; however, it still managed to adhere to the maximum ASTM freeze point limit of −47 °C. The mixture consisted of 90% C_9–C_{15} mixture components, which is similar to the carbon number distribution of conventional jet fuel. Optimisation of jet fuel to meet the specified freeze point and viscosity criteria consequently only allows for the presence of 10% C_{16}–C_{18} mixture components. Whilst the quantity of C_{16}–C_{18} mixture components may seem insignificant, it will make a significant contribution towards increasing jet fuel production volumes.

Conclusions

The proposed viscosity model was able to accurately predict the viscosities of new jet fuel blends in the C_9–C_{18} carbon number range. Even though the model was constructed by making use of viscosity measurements at 20 °C, it was possible to produce jet fuels which possessed

viscosities in the region of the 4.5 cSt at − 20 °C limit proposed by the ASTM, demonstrating that the ASTM D341 conversion performed during construction of the model was successful.

It was apparent that the validation of the model for freeze point produced unsatisfactory results. The Freeze point can be defined as the temperature at which a liquid changes to a solid when cooled slowly. Molecules in the liquid state are randomly organised, but when the molecules crystallise into the solid state, they become more ordered, forming a crystal lattice [21]. Freeze point is influenced by the strength of the crystal lattice [22]. The strength of the crystal lattice in turn, is controlled by various factors, including:

- Molecular symmetry [23] [22]; and
- Intermolecular forces [24] [23].

The major flaw of the experimental observations and the developed model was that it could account neither for the strength of the crystal lattice, nor for the fact that many organic molecules crystallise in different crystal structures (polymorphism). Maddox [25] found that as little as 0.5–1.0% of precipitated wax may be sufficient to cause gelation of fuel, which indicates that freeze point cannot be determined fully by only the bulk properties of the fuel. Freeze point is intrinsically a crystallisation phenomenon, in which the random presence of trace amounts of molecules and "seeding" nuclei may play an important role.

If the effects of crystal formation were disregarded, it could be concluded that the ideal *i*:*n* mass ratio and carbon number distribution for jet fuels with a maximum viscosity of 4.5 cSt at − 20 °C and a maximum freeze point of − 47 °C, is as presented in Table 4. Furthermore, if the aim was to minimise both freeze point and viscosity, the ideal *i*:*n* mass ratio would be 1:0 and the mixture would consist largely of C_9–C_{11} mixture components. However, if the model was able to account for crystal formation, the ideal *i*:*n* mass ratio as well as the ideal carbon number distribution of the above mentioned optimisation studies may have differed. From the results obtained it is evident that *i*:*n* mass ratio and carbon number distribution cannot be treated as two separate entities. Altering either of these compositional parameters would impact on the remaining parameter. To adhere to the freeze point specification maximum, the carbon number distribution of jet fuel mixtures would have to be decreased and the relative proportions of the C_9–C_{11} components should be increased as the *n*-paraffin content of the mixtures is increased.

This study considered only the low-temperature fluidity properties of jet fuel and disregarded other physical properties, which are also critical for the correct functioning of turbine engines. If physical properties, such as flash point, density and D86 boiling point distribution had been considered, the ideal i:n mass ratio and carbon number distribution ranges specified might also have differed from the ones currently prescribed. Furthermore, ASTM D7566 [26] stipulates that jet fuels containing synthesised hydrocarbons must contain at least 8% aromatic compounds; if this minimum specification was taken into consideration, the i:n mass ratio and carbon number distribution ranges specified might also have differed from the ones currently recommended.

Development of accurate freeze point regression models will remain a futile task until molecular descriptors adequately describing crystal formation of the molecules present in jet fuels can be established.

References

1. NASA (2002) Celebrating a century of flight. NASA, Washington, DC
2. Schäfer AW (2016). The prospects for biofuels in aviation (Chap. 1). In: Chuck C (ed) Biofuels for aviation: feedstocks, technology and implementation. Elsevier Inc., Amsterdam
3. Eller Z, Varga Z, Hancsók J (2013) Production of jet fuel from renewabe source material. Chem Eng Trans 35(2):1057–1062
4. Chuck CJ (2016). In: Chuck C (ed) Biofuels for aviation: feedstocks, technology and implementation. Elsevier Inc., Amsterdam
5. Chuck CJ, Mc Manus M, Allen MJ, Singh S (2016) Biofuels for aviation: feedstocks, technology and implementation. Elsevier Inc., Amsterdam
6. Corporation Chevron (2006) Alternative jet fuels. Chevron Corporation, San Ramon
7. de Klerk A (2016) Biofuels for aviation: feedstocks, technology and implementation. Elsevier Inc., Amsterdam
8. Agee MA (1997) Economic conversion of natural gas to synthetic petroleum liquids. https://web.anl.gov/PCS/acsfuel/preprint%20archive/Files/42_2_SAN%20FRANCISCO_04-97_0672.pdf. Accessed 10 Feb 2016
9. Coordinating Research Council (2010) Develop an aviation fuel cold flow flowability test to replace freezing point measurement. CRC, Alpharetta
10. ASTM (2016) ASTM D1655-16c: standard specification for aviation turbine fuels. ASTM, Pennsylvania
11. de Klerk A (2008) Fischer–Tropsch refining, Pretoria: UP (Thesis-PhD)
12. Cornell JA (2002) Experiments with mixtures: designs, models, and the analysis of mixture data. Wiley, Hoboken
13. Atkinson AC, Donev AN, Tobias R (2007) Optimum experimental designs, with SAS. Oxford University Press, Oxford
14. Coetzer RLJ, Haines LM (2013) Optimal designs for multiple-mixture by process variable experiments. In: Uciński P, Atkinson AC (eds) mODa 10—advances in model-orientated design and analysis. Springer, New York, pp 45–53
15. Goos P, Jones B, Syafitri U (2016) I-optimal design of mixture experiments. J Am Stat Assoc III:899–911

16. Stat-Ease Inc (2015) Design-expert software. Stat-Ease Inc, Minneapolis
17. ASTM (2009) ASTM D341-09: standard practice for viscosity-temperature charts for liquid petroleum products. ASTM, Pennsylvania
18. Affens WA, Hall JM, Holt S, Hazlett RN (1984) Effect of composition in freezing points of model hydrocarbon fuels. Elsevier 63(4):543–547
19. Coetzer RLJ, Rossouw RF, Lin DKJ (2008) Dual response surface optimisation with hard-to-control variables for sustainable gasifier performance. J R Stat Soc Ser C Appl Stat 57(5):587–657
20. Derringer G, Suich R (1980) Simultaneous optimisation of several response variables. J Qual Technol 12:214–219
21. ASTM DS 4B (1991) Physical constants of hydrocarbons and non-hydrocarbon compounds. ASTM, Pennsylvania
22. Flack H, Gavezzotti A (2005) Crystal packing. International Union of Crystallography, Chester
23. Katrizki A, Kuanar M, Slavov S, Hall C, Karelson M, Kahn L, Dobchev D (2010) Quantitative correlation of physical and chemical properties with chemical structure: utility of prediction. Chem Rev 110(10):5714–5789
24. Brown TL, LeMay E, Bursten BE (2006) Chemistry, the central science, 10th edn. Pearson Education Inc, New Jersey
25. Maddox J (2012) Cold flow additives. Infineum, Milton Hill
26. ASTM D7566-15c (2015) Standard specification for aviation turbine fuel containing synthesised hydrocarbons. ASTM, Pennsylvania